Manipulating oxygen sublattice in ultrathin cuprates: A new direction to engineer oxides

Debakanta Samal[a),c)] and Gertjan Koster[b)]
Inorganic Materials Science Group, MESA+ Institute for Nanotechnology, University of Twente, 7500 AE, Enschede, The Netherlands

(Received 12 June 2014; accepted 17 November 2014)

Atomic engineering of complex oxide thin films is now reaching a new paradigm: the possibility to control the cation coordination by oxygen anions. Here, we show two examples of stabilization of novel structural phases by manipulating the oxygen sublattices in complex Cu-based oxide thin films grown on $SrTiO_3$: (i) epitaxial strain stabilization of a near cubic form of CuO and (ii) thickness-dependent structural transformation from bulk planar (polar) to chain-type (nonpolar) in $SrCuO_2$ thin films that relieves the electrostatic instability. Experimental investigation on ultrathin CuO layer identifies the existence of an elongated ($c/a \sim 1.34$) rocksalt-type CuO phase, pointing to metastable 6-fold coordinated Cu with the hole occupied in the $3d_{x^2-y^2}$ orbital. For ultrathin $SrCuO_2$ layers, we demonstrate the possibility of moving oxygen ion from CuO_2-plane to Sr-plane forming chain-type structure. X-ray absorption spectroscopy reveals preferential hole-occupation at the Cu-$3d_{3z^2-r^2}$ orbital for chain-type structure unlike to the planar case. Our findings testify unique stabilization processes through atomic rearrangement and provide new insight into the experimental realization of novel cuprate-hybrids to look for exciting electronic properties.

I. INTRODUCTION

Oxide materials, starting from simple binary to more complex ternary compounds, exhibit a wide variety of electronic and ionic properties. With the advent of atomically controlled oxide thin film growth,[1,2] many different artificial structures such as titanate superlattices (SLs)[3] or magnetic/superconducting heterostructures[4–6] have been fabricated in the last two decades with the aim to systematically vary the cation stoichiometry across the thickness of the film that in the search for modified and new physical phenomena. Most notably, since the functionality in electronic and magnetic devices is directly derived from particular properties at interfaces in hetero-epitaxial systems (*the famous quote by Nobel Laureate Herbert Kroemer states: "the interface is the device"*), the studies involving oxide interfaces are on high demand and rapidly progressing. The last decade has witnessed explosive growth of research on various oxide heterostructures resulting in the discovery of exciting interfacial phenomena.[7–9] In most cases, the designed interfaces are formed and defined by the alternation of cationic species, with the assumption that the oxygen sublattice will adapt accordingly. However, in very recent works, more attention has been given to control and subsequently measure oxygen sublattice in oxide thin films/heterostructures, which we know to play a pivotal role in the chemical-bonding and structure–property relation. The crystallographic mismatch, violation of local charge neutrality, and the difference in chemical potentials between the constituents belonging to thin films/heterostructures can strongly affect the atomic and therefore electronic structure referenced with its bulk counterpart.

The most studied effect of epitaxy on the oxygen sublattice can be found in ABO_3 perovskite oxides, which are greatly influenced by the distortion of the BO_6 octahedral network that arises either due to change in lattice symmetry or due to orbital degeneracy (Jahn–Teller effect). The distortion in general can be of three types: (a) cation displacement within octahedra, (b) deformations (changes in the size of the octahedra), and (c) co-operative tilting (rotations) of the octahedra. Primarily, in thin films/heterostructures, the lattice symmetry mismatch between the substrate and film/between different films belonging to heterostructures introduces octahedral distortion at the interface.[10–14] Schematics of octahedral tilt pattern and various possible deformation modes that can occur at the interface to accommodate the lattice distortion are shown in Fig. 1. A recent study by Aso et al.[12] found a significant

Contributing Editor: Amit Goyal
Address all correspondence to these authors.
[a)]email: deb.samal2002@gmail.com
[b)]email: g.koster@utwente.nl
[c)]Presently at Max Planck Institute for Solid State Research, Stuttgart, Germany
This paper has been selected as an Invited Feature Paper.
DOI: 10.1557/jmr.2014.391

 © Materials Research Society 2014

https://doi.org/10.1557/jmr.2014.391 Published online by Cambridge University Press

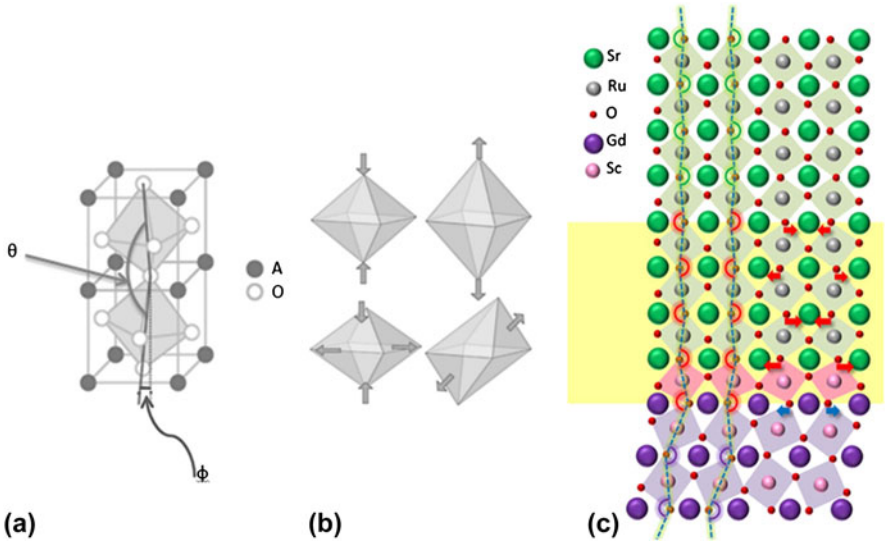


FIG. 1. (a) Schematic of the octahedral in-plane rotations (φ) and out-of-plane tilts (θ) and (b) various modes of octahedra deformation that can occur at the heterointerface to accommodate the lattice distortion. (c) Structural model around heterointerface between the SRO thin film and $GdScO_3$ (GSO) substrate. The termination layer of the GSO substrate is a ScO_2 layer and the first layer of the SRO epitaxial thin film is a SrO layer, where ScO_6 octahedra (pink squares) at the hetero-interface share oxygen atoms in the SrO layers. Blue dashed lines represent the oxygen octahedral tilt angles. Red and blue arrows represent the oxygen atomic shifts from that of the bulk SRO and GSO, respectively. The yellow box in the vicinity of the heterointerface represents the region where the tilt angle mismatch is accommodated. [Image (c) is taken from Ref. 12.]

distortion in terms of octahedral tilt at the heterointerface between a $SrRuO_3$ (SRO) film and a $GdScO_3$ (GSO) substrate and that remarkably persists up to several atomic layers at the interface [Fig. 1(c)]. This observation emphasizes the fact that the structural mismatch at the heterointerface in oxide heterostructures can be accommodated by the rearrangement of oxygen sublattice. For the case of magnetic perovskite oxides such as manganites, ruthenates, and nickelates, the electronic transport and magnetic properties sensitively depend on the B–O–B bond angle and B–O bond length.[15,16] This is because the electron hopping matrix element (t_{ij}) and superexchange interaction (J) strongly depend on both the above parameters. Therefore, by controlling the oxygen octahedral distortion and their connectivity and coupling across the perovskite oxide interfaces, one can indeed demonstrate the tunability of oxide thin film properties over a wide range, and moreover it can provide an ideal platform to investigate the interplay between spin, orbit, and lattice degree of freedom in oxide materials at the atomic scale.[11,13] Indeed, lattice deformation induced metallicity has been reported in $LaTiO_3$ thin films, which otherwise is a correlated Mott insulator in the bulk phase.[17] Concerning magnetism, it was shown ultrathin $La_{0.7}Sr_{0.3}MnO_3$ films grown on $SrTiO_3$ that the Curie temperature can be significantly enhanced by epitaxial strain which imposes a different octahedral rotation pattern.[18] First principles calculation even suggests the possibility for unexpected ferroelectricity in $PbTiO_3/SrTiO_3$ heterostructure, arising from octahedral rotation coupling at the interface.[19] Though, the octahedral rotation/tilting/deformation at the interface due to lattice symmetry mismatch is believed to induce novel physical phenomena in thin films/heterostructure systems, a complete atomic scale understanding of such phenomena is still missing until now. This is because of the experimental challenges that require the precise measurements of the position of both cations and oxygens. While in the examples given above, subtle changes in the oxygen sublattice are being explored, more dramatic changes in properties are expected when the cation coordination can be affected and controlled.

The research addressed in this paper involves the control of the oxygen sublattice in such a way that the coordination of cations, here copper, in the structure is varied from 4-fold to 6-fold, and in-plane to out-of-plane configuration respectively by means of thin film methods. First, we discuss the possibility to stabilize a near cubic (tetragonal) form of CuO by using epitaxial strain,[20,21] thereby increasing the Cu coordination from 4 to nearly 6 [Fig. 2(a)]. Indeed, earlier studies on various cuprate thin films suggest that the lattice mismatched strain can have profound effect on oxygen sublattice reorganization and also can even drive structural transition when the film is below certain thickness.[23–25] The structure of bulk CuO as found in nature is unique and at variance with other 3*d* transition-metal monoxides (TMMOs). While MnO, FeO, CoO, and NiO all crystalize in the rock-salt crystal structure with small lattice distortion (<2%) at low temperature,[26–29] CuO crystalizes itself in a noncentrosymmetric monoclinic structure possibly due to strong Jahn–Teller distortion.[30] From a magnetic point of view, CuO exhibits an insulating antiferromagnetic ground state similar to other TMMOs. However, while

https://doi.org/10.1557/jmr.2014.391 Published online by Cambridge University Press

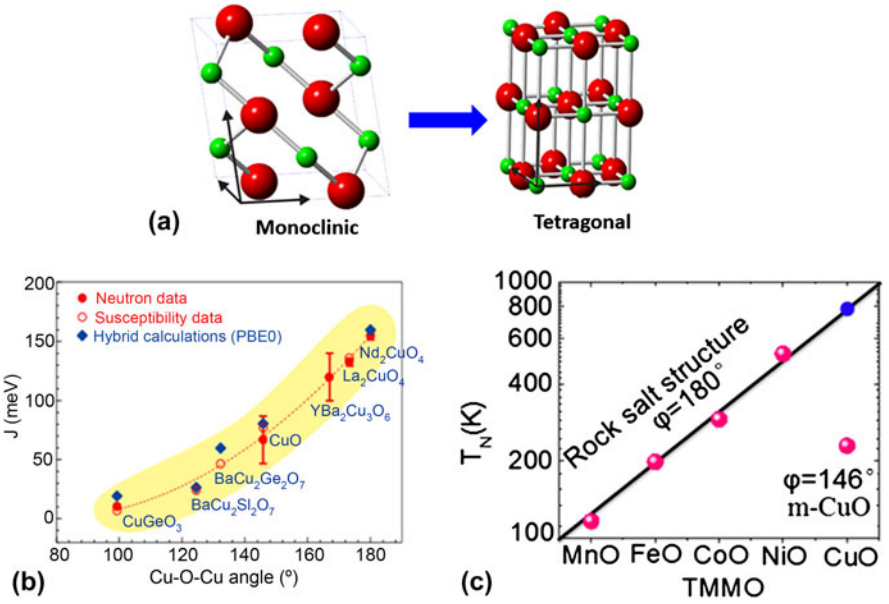


FIG. 2. (a) A schematic overview of the change in unit cell symmetry from bulk monoclinic (a = 4.68373 Å, b = 3.4226 Å, c = 5.1288 Å, and β = 99.54°) to strain induced tetragonal (a = 3.91(2) Å and c = 5.25(10) Å) CuO. The green and red colored atoms represent oxygen and copper, respectively. (b) Principal superexchange interaction as a function of the Cu–O–Cu bond angle for various low-dimensional cuprates [Figure (b) is taken from Ref. 22]. (c) Néel temperatures for TMMOs. The blue dot represents the possible Néel temperature that could emerge for rocksalt type CuO assuming a linear trend.

the other TMMO members exhibit a linear trend of increasing Néel temperatures (T_N) with increasing atomic number (MnO:T_N = 118 K, FeO:T_N = 200 K, CoO:T_N = 291 K, and NiO:T_N = 523 K),[29] the monoclinic CuO (m-CuO) shows a substantial departure from this trend having relatively lower T_N. Note that it exhibits two distinct antiferromagnetic phases: (i) commensurate collinear and (ii) incommensurate spiral structures with T_N = 213 and 230 K, respectively.[31] The reduction of T_N is believed to be related to reduced effective J due to the lower Cu–O–Cu bond angle (ϕ = 146°) of the monoclinic structure. Since J strongly depends upon the Cu–O–Cu bond angle as shown in Fig. 2(b) for various low dimensional cuprates,[22] one would expect that if CuO were found in the high-symmetry rocksalt structure or perhaps a closely related tetragonal structure with the Cu–O–Cu bond angle (ϕ = 180°), then T_N would be largely enhanced up to ~800 K assuming the linear trend as shown in Fig. 2(c). Indeed, first principles calculation predicts T_N up to 800 K for the rocksalt-like CuO,[32,33] and more interestingly, a very recent study on CuO–Cu_2O heterostructures obtained by high-temperature annealing of copperplate reports the T_N close to 600 K, which possibly could be due to high-symmetry CuO phase.[34] Since the interplay of superconductivity and magnetism is a key issue and there exists experimental evidences for strong antiferromagnetic superexchange interaction in both the insulating parent phase and the doped superconducting phase of cuprates,[22] the study of the high-symmetry CuO phase with possible large antiferromagnetic coupling would be an ideal model system to investigate the correlated physics that lies at the heart of high-T_c cuprate superconductivity. Moreover, the original proposal by Bednorz and Muller stated that a highly symmetric divalent copper monoxide with partially filled e_g orbital would undergo Jahn–Teller (JT) distortion and consequently can have strong electron–phonon interaction based on the JT polaron model, which might mediate superconductivity.[35] From the above consideration, the study on highly symmetric (cubic/tetragonal) CuO is highly instructive and might elucidate the fundamental factors underlying high-T_c superconductivity in cuprates.[36]

Second, we address a method that originated from the studies involving the interfaces between polar and nonpolar band insulators (e.g., $LaAlO_3$ (LAO); polar and $SrTiO_3$ (STO); nonpolar) that have revolutionized our traditional understanding of interfacial effects and spurred a flurry of research activities. Various intriguing phenomena such as 2D electron gas,[37,38] superconductivity,[39] magnetism,[40,41] and electron–hole liquid behavior[42] have been reported to emerge at LAO/STO interfaces. Akin to $LaAlO_3$, the infinite-layer (IL) tetragonal $SrCuO_2$ (a = b = 3.926 Å, c = 3.432 Å)[43] is also an example of a polar system.[44] In fact, $SrCuO_2$ (SCO) can be synthesized in both tetragonal and orthorhombic phases. The orthorhombic phase acts as an ideal 1D quantum magnetic system to investigate fundamental physical phenomena such as 1D

https://doi.org/10.1557/jmr.2014.391 Published online by Cambridge University Press

Mott insulator and spin–charge separation.[45–47] The IL tetragonal phase of SCO [Fig. 3(a)] with its 2D CuO_2 planes is widely known to be a parent structure for high-T_c cuprate superconductors.[49–51] The high-T_c superconductor can be derived from IL structure, by insertion of chemically distinct metal-oxide layers parallel to CuO_2 layers. Its structure can be considered as an oxygen deficient perovskite, with Cu^{2+} ions coordinated to four equatorial O^{2-} ions and no O^{2-} ions in the Sr^{2+} plane/along the apical direction surrounding Cu ions [Fig. 3(a)]. Since each alternative constituent atomic plane has a formal charge of $\pm 2e$, it leads to a built-in electrostatic potential, which increases with the SCO thickness as shown in Fig. 3(c). The alternating layers with a nominal charge of $\pm 2e$ (in a purely ionic model) cause a build-up of electrostatic energy of $\sim$8 eV per unit-cell (uc) of SCO. This value constitutes a strong electrostatic instability and makes the IL structure highly polar. For very thin films of such materials, electronic charge transfer, which is a monotonic function of thickness, does not appear to be sufficient to quench the electrostatic instability.[52] Rather, a structural transformation involving the displacement of lighter atoms turns out to be the preferred mechanism. However, for relatively thick films, this instability can possibly be relieved by extrinsic defects (oxygen vacancy, intermixing) and/or charge transfer. Indeed, theoretical studies predict that the polarity of nanoscale objects and ultrathin films can be avoided by a structural transformation involving atomic rearrangements.[52–55] In particular, the study by Zhong et al.[52] on IL cuprates predicts a transformation from the bulk planar to a chain-type structure for ultrathin films of about 5 uc thick. The resulting chain-type structure incorporates an O^{2-} ion in the Sr^{2+}-plane as opposed to the planar structure and thus consists of charge neutral SrO^0 and CuO^0 layers [Fig. 3(b)]. Alternatively, this can be viewed as if the CuO_4 plaquettes are stacked along a perpendicular direction as compared to that of planar case. The movement of an O^{2-} ion to the Sr^{2+}-plane reduces the anisotropy of the structure and holds apical oxygen surrounding the Cu^{2+} ions. In the process of such rearrangement of oxygen ions, the *c*-axis lattice parameter of the chain-type SCO increases by 0.5 Å as compared to the bulk-planar counterpart due to the associated Cu–O bonding in the *c*-direction. In essence, the stabilization of the ultrathin film structure involves a subtle compromise between two energy terms; namely the elastic strain energy and the electrostatic polarization energy. Eventually, at the expense of considerable amount of elastic strain energy, the system lowers its electrostatic potential energy and makes the chain-type structure to be energetically most favorable in the ultralow thickness limit. It has to be mentioned here that the realization of artificially made chain-type structures in ultrathin SCO layers will open new routes to design/engineer novel superconducting cuprate-hybrids, with alternation of chain and plane-type structures that lies at the heart for the structural model of high-T_c cuprate superconductors. Indeed, a recent study by us reveals that an ideal combination (comprising of chain and plane-type CuO blocks stacked along the *c*-direction) of heterostructure design is essential to tune the electronic properties toward superconducting phase in cuprate hybrids.[56] Moreover, the study by Huijben et al. suggests that the addition of a $SrCuO_2$ epilayer strongly reduces the impurity scattering at the conducting interfaces in oxide $LaAlO_3$–$SrTiO_3$ heterostructures, as shown by the observation of higher carrier mobilities.[57] Most interestingly, the observation by Castro et al.[58] of high-temperature (up to 40 K) superconductivity in $CaCuO_2/SrTiO_3$ SLs grown in highly oxidizing condition has drawn immense interest to IL based cuprate heterostructures.

In the second part of this paper, we show that an atomic rearrangement of oxygen ions occurs within SCO layers below a certain thickness to alleviate the associated

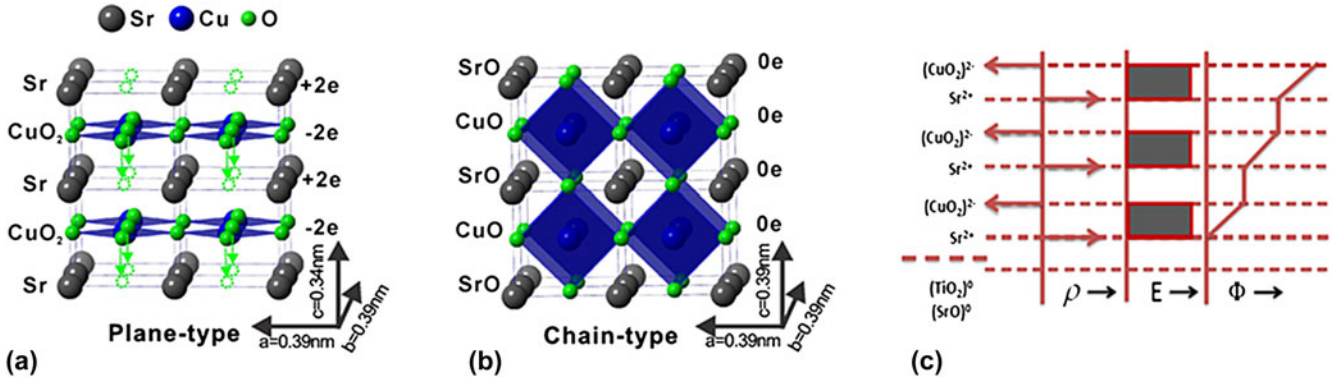


FIG. 3. Schematics of the (a) planar and (b) chain-type crystal structures for tetragonal SCO. For clarity, we indicate the oxygen displacement by arrows in (a) that transforms the planar structure into chain-type [Figures (a) and (b) are taken from Ref. 48] and (c) represents stacking sequence of constituent layers with alternating net charge (ρ) for plane-type SCO layer grown on STO substrates (electric field (***E***) and the built in potential (ϕ) profiles associated with planar structure are also shown).

https://doi.org/10.1557/jmr.2014.391 Published online by Cambridge University Press

electrostatic instability due to their polar nature. We study SCO/$SrTiO_3$ SLs as well as single SCO layers grown on STO by pulsed laser deposition (PLD). Our findings based on structural and spectroscopic investigation unambiguously demonstrate a transformation from planar to chain-type structure in ultrathin films of SCO.[48,59] Besides being an interesting model system to study such dramatic structural changes and their formation pathways, we demonstrate that the oxygen sublattice can be effectively engineered by systematic variation of the individual sublayer thicknesses in the SL, giving each layer a specific function, for example, current-carrying layers, charge reservoirs, and scaffolding layers. In a simple picture, the structural paradigm of high-T_c cuprate superconductors is built on current carrying CuO_2 planes (where the Cu ion is co-ordinated to 4 in-plane oxygen) separated by charge reservoir blocks that essentially dope the CuO_2 plane giving rise to superconductivity. Charge carriers are generally added to the CuO_2 plane either by cation substitution (like Sr^{2+} in $La_{2-x}Sr_xCuO_4$) or by addition of oxygen as in the case of $YBa_2Cu_3O_7$.[60] The additional oxygen incorporated forms Cu–O chains and acts as a charge reservoir by attracting electrons from the CuO_2 plane. The plane comprising of Cu–O chains possesses apical oxygen unlike the current carrying CuO_2 plane. Based on the above structural model, the IL compound $ACuO_2$ (A = Ca, Sr, or Ba) appears to be the simplest structure that holds key ingredients for realizing high-T_c superconductivity. Designing heterostructures made out of ILs and controlling the oxygen co-ordination from in-plane to out-of-plane (plane to chain type) on the atomic scale as has been illustrated in this article might provide new ways to mimic the basic structural model and artificially fabricate high-T_c cuprate superconductors without resorting to any chemical substitution. Indeed, the earlier work by Balestrino et al.,[61,62] Castro et al.,[58] and Norton et al.[63] reports the observation of high-T_c superconductivity in IL based hybrids; however, a detailed understanding of the oxygen sublattice reorganization as a function of film thickness in such polar systems was missing.

II. EXPERIMENTAL DETAILS

SCO/STO SLs as well as single layers of SCO and CuO thin films were grown on TiO_2-terminated (001)-oriented STO substrates by PLD, using a Twente Solid State Technology (TSST) system and a 248-nm-wavelength KrF excimer laser (LPX 200 from Germany Coherent, Inc.). The most homogeneous part of the laser beam was selected using a 4 × 15 mm rectangular mask and an image of the mask was created on the stoichiometric targets (CuO, $SrTiO_3$, and $SrCuO_2$) with a lens. Before deposition, the target was preablated for 2 min at a pulse rate of 5 Hz and a laser fluence of 2 J/cm^2. The substrate temperature during the growth was set at 650 °C and the oxygen partial pressure was maintained 0.3 mBar. The deposition was carried out at a pulse rate of 1 Hz and a laser fluence of 2 J/cm^2. After the deposition, the samples were cooled to room temperature at a controlled cooling rate of 10 °C/min. These deposition conditions were optimized to result in the growth of the tetragonal phase of SCO and CuO. Reflection high-energy electron diffraction (RHEED) was used to monitor the growth and control the thickness of SLs with uc precision. Figure 4(a) shows the RHEED intensity oscillations during the growth of individual layers (CuO, SCO, and STO) indicating the layer-by-layer growth mode. To grow complete stack of SL structures, the number of laser pulses required for each layer of a specific material was calibrated and then the growth was performed in accordance with the periodicity of SL structure. In Figs. 4(b) and 4(c), we show typical streaky RHEED pattern after the growth of $[((SCO)_3/(STO)_2)_{20}]$ and $[((SCO)_8/(STO)_2)_{20}]$ SLs, respectively, signifying 2D growth. The structural characterization of the samples was carried out using x-ray diffraction (XRD), x-ray photoelectron diffraction (XPD), high-resolution scanning transmission electron microscopy (STEM) and composition by electron energy loss (EEL) spectroscopy. High-angle annular dark-field (HAADF), annular bright field (ABF) STEM images, and EEL spectra were acquired using a FEI Titan^3 80-300 microscope, equipped with a double aberration corrector.

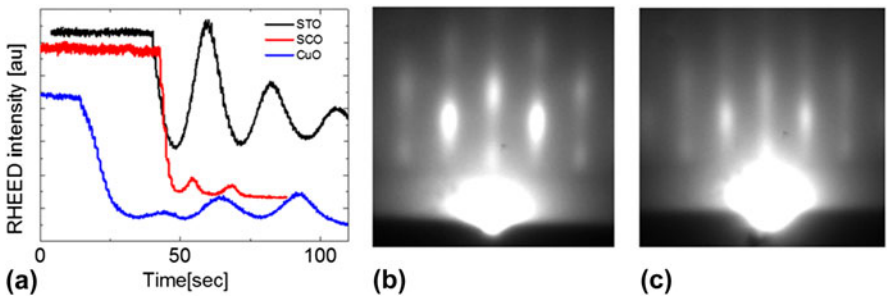


FIG. 4. (a) RHEED intensity variation during the growth of individual layers (plots are shifted vertically for clarity). Streaky 2D-like RHEED pattern observed at the end of the growth of (b) $[((SCO)_3/(STO)_2)_{20}]$ and (c) $[((SCO)_8/(STO)_2)_{20}]$ SLs, respectively.

https://doi.org/10.1557/jmr.2014.391 Published online by Cambridge University Press

The ABF/ADF images were recorded with an annular detector capturing scattering from 26 to 60 and from 15 to 24 mrad, respectively. The elastic scattering image simulations were obtained using STEMSIM.[64] The ionic valence state of Cu was determined by x-ray photoelectron spectroscopy (XPS). Polarized x-ray absorption (XA) spectra were acquired at a beam line of 4.0.2 at the advanced light source in total electron yield mode by monitoring the sample drain current. To avoid charging effects during the XA measurement, the samples for this purpose were grown on Nb-doped (0.05 at.%) STO substrates.

III. RESULTS AND DISCUSSIONS

A. Forced epitaxy induced rocksalt type CuO: A new member in the 3*d* TMMO series

In this section, we discuss about the structural and electronic properties of ultrathin rocksalt type tetragonal CuO (t-CuO) film grown on STO. The induced epitaxial strain from the STO substrate is found to be the underlying factor in stabilizing the tetragonal phase of CuO when the layer thickness is limited to few uc. In situ monitoring of the growth of the CuO films using RHEED demonstrates a transition of the film structure as the film thickness increased (Fig. 5). In the initial part of the growth, we clearly observe a RHEED pattern with elongated spots and not showing reflections characteristic for 3D islands [Figs. 5(a) and 5(b)], which corresponds to the tetragonal structure of CuO.[20,21] However, as the growth continued, 3D spots gradually appear [Figs. 5(c) and 5(d)], which are presumed to emerge when the film relaxes to its bulk monoclinic phase. In most cases, elongated RHEED patterns were observed when the thickness of the CuO films was limited to a maximum up to 5 uc as monitored by RHEED oscillations. To ensure the growth of a pure CuO phase without the formation of other copper oxide phases (e.g., Cu_2O, Cu_3O_4), we examined Cu valence state using XPS. Distinct satellite structure corresponding to the Cu $2p_{3/2}$ peak [Fig. 5(e)] indicates that copper ions have a formal valence of +2 as expected for CuO and unlike Cu_2O.[21]

Detailed STEM was carried out to provide further insight into the structure of the ultrathin CuO films. To avoid any damage to the ultrathin CuO film during ion beam processing, it was capped with 20 uc of crystalline STO. Figure 6 shows a HAADF-STEM image for the same along the [100] direction in which the atomic columns of the heavy elements (e.g., Cu, Ti, and Sr) show up as bright spots. The middle CuO layer grows epitaxially with respect to the STO substrate with an atomic arrangement consistent with the projection of the rocksalt structure shown schematically on the left side of Fig. 6. Using the lattice parameter of the STO substrate (a = 3.905 Å) as an internal calibration, we find a- and c-axis lattice parameters of CuO to be of 3.91(2) and 5.25(10) Å, respectively, suggesting an elongated rocksalt type structure. To know the arrangement of the oxygen atoms on a local scale, we carried out ABF-STEM imaging. ABF-STEM imaging collects the low-angle scattered electrons unlike HAADF-STEM which collects electrons scattered to higher angles. As a consequence, ABF-STEM is more sensitive to the light atoms like oxygen whereas HAADF-STEM mostly maps the heavy atoms.[65] Therefore, the combination of both ABF-STEM and ADF-STEM provides a unique opportunity to simultaneously monitor the position of the oxygen atoms with respect to heavier (Cu, Sr, and Ti) atoms.[12] Figure 7(b) shows a simultaneously acquired ABF image (intensity inverted to make the atoms appear as white

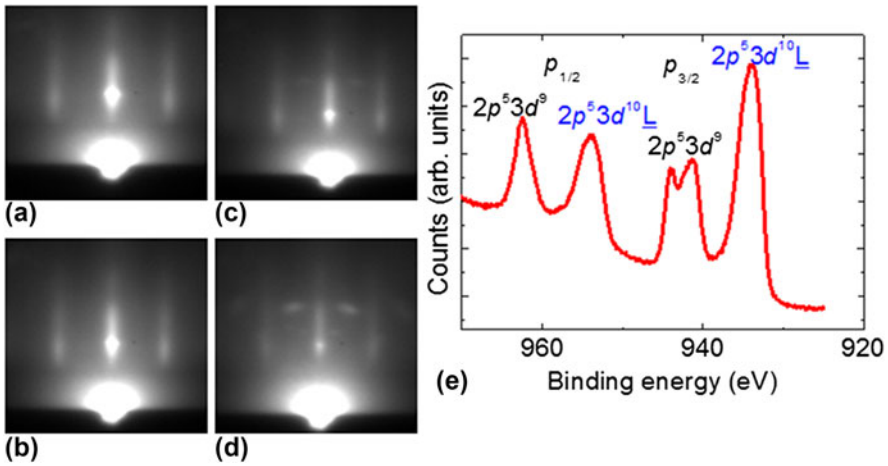


FIG. 5. Evolution of the RHEED pattern [(a) → (b) → (c) → (d)] during the growth of CuO on STO that clearly shows the transition from a streaky pattern [(a) and (b)] to the onset of 3D spots [(c)] and [(d)]; (a), (b), (c), and (d) correspond to the RHEED pattern after ~3, 4, 5, and 8 uc of CuO growth, respectively. (e) The Cu 2*p* core-level XPS spectrum for a CuO film indicating Cu^{2+} state.

https://doi.org/10.1557/jmr.2014.391 Published online by Cambridge University Press

spots on a dark background) together with its ADF image [Fig. 7(a)] of the CuO film and its neighboring STO layers along the [110] direction. Comparison of ADF and ABF images reveals extra oxygen atomic columns between two Ti columns of STO film [Fig. 7(b)]. Indeed, the ABF image corresponding to the CuO layer also shows extra columns belonging to the oxygen positions lying between two Cu columns. To improve the visibility of the oxygen columns, the intensity-inverted ABF image (in green) is superimposed with the ADF image (in red). The columns containing heavy elements together with oxygen ions are visible as yellow (overlay of red and green) dots whereas the columns containing only oxygen ions are visible in green. We clearly observe the presence of oxygen columns between the heavy Ti columns in the STO layer and between the heavy Cu columns in the CuO layer. This directly confirms the arrangement of the oxygen ions in the CuO layer as illustrated in Fig. 2(a) for the tetragonal CuO. Since the ABF images contain the information of both the heavy and light elements and the ADF only contain that of the heavy elements, the ABF image can be divided by its corresponding ADF image to enhance the visibility of the light elements further. This divided image (in green) was combined again with the ADF image (in red) [Fig. 7(c), inset], which nicely shows the light atomic columns in green and the heavy ones in red. The average O–Cu–O bond angle estimated from the image is found to be 180 ± 2°. The simulated image assuming the structural model agrees well with the experimental result as shown in Fig. 7(d).

To probe the electronic structure and symmetry of the unoccupied Cu 3*d* orbital for the novel tetragonal phase of CuO, we performed XA spectroscopy using linearly polarized x-rays. In these measurements, electrons are excited from a selected core shell to an empty state of the absorbing transition metal upon the irradiation of x-rays with the appropriate resonance energy. The transition intensity scales with the number of empty states being probed. Since the orientation of the *p* and *d* orbitals is not spherically symmetric in space, the probability of an

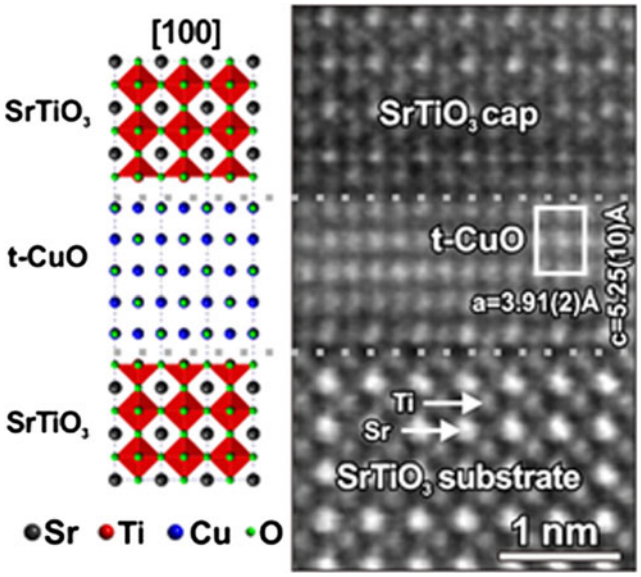


FIG. 6. HAADF-STEM images along the [100] direction. A tetragonal structure model matching the observations is shown on the left side. [Image is taken from Ref. 20.]

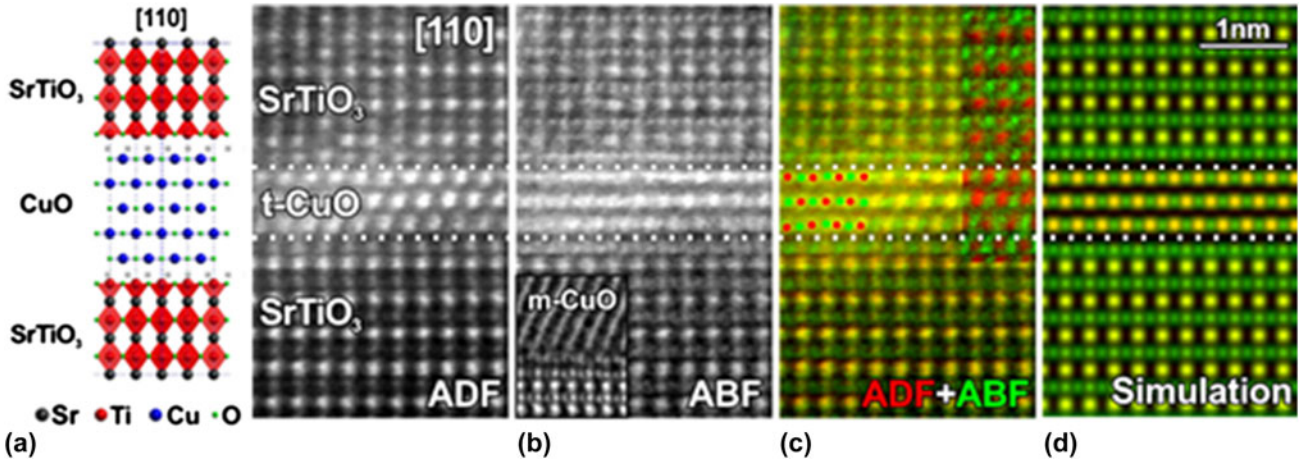


FIG. 7. (a) ADF image showing the atomic columns of the heavy atoms along the [110] direction (Sr, Ti, and Cu). (b) The reversed ABF image acquired simultaneously with the ADF image shows the atomic columns of light elements (oxygen) together with those of heavy elements. The inset shows a reversed ABF image of a thicker CuO film on the STO substrate. It has collapsed to its ordinary monoclinic structure which is clearly different from the tetragonal structure of ultrathin CuO film. (c) Combined color map with ADF in red and reversed ABF image in green. The heavy element columns together with oxygen were combined to be yellow after color mixing while the O columns remain green. The inset is a combined color map with the ADF image in red and oxygen-enhanced ABF image in green. The Cu and O positions are illustrated with red and green disks on the left of the CuO layer. (d) Simulation of the ADF and the reversed ABF images. A tetragonal structure model along the [110] direction is shown on the left hand side. [Image is taken from Ref. 20.]

https://doi.org/10.1557/jmr.2014.391 Published online by Cambridge University Press

electron transition strongly depends also on the orientation of the ***E*** vector of the linearly polarized x-rays with respect to the Cu–O coordination and the films' crystalline axes. By changing the direction of the x-ray polarization (***E*** vector) relative to the sample surface, one can probe the angular dependence of the empty valence states. Therefore, using vertically or horizontally polarized x-rays oriented along the in-plane [100] direction (i.e., the ***E*** vector aligned along the in-plane [010] direction and canted out-of-plane by 30° relative to the [001] direction) in grazing incidence geometry, we can probe in-plane $d_{x^2-y^2}$ or the out-of-plane $3d_{z^2}$ orbitals at the Cu site, respectively.

Since the Cu ion in case of tetragonal CuO is surrounded by an elongated oxygen octahedron ($c/a > 1$), the e_g orbitals ($d_{x^2-y^2}$, d_{z^2}) split to remove the orbital degeneracy as schematically shown in Fig. 8(b). This orbital configuration arises because the elongation along the *c*-axis lowers the Coulomb energy associated with the electrons in the $3d_{z^2}$ orbital. Therefore, the hole [$Cu^{2+}(d^9)$] at the Cu site is expected to be localized at an e_g $d_{x^2-y^2}$ orbital for this novel phase, similar to what is generally observed in the case of high-T_c cuprate members. In Fig. 8(c), we show XA spectra for the tetragonal CuO films at the Cu $L_{2,3}$ edges with the ***E*** vector aligned in-plane or canted out-of-plane. The peaks at the Cu $L_{2,3}$ edges (i.e., at about 930 and 950 eV) correspond to transitions from the Cu $2p_{3/2}$ to Cu 3*d* and Cu $2p_{1/2}$ to Cu 3*d* orbitals, respectively. These transitions are commonly referred to as $2p^6 3d^9 \rightarrow 2p^5 3d^{10}$, where an electron from the Cu 2*p* orbital is promoted to the 3*d* orbital after absorbing a photon.[58,66–69] We observe a strong dependence of the spectral intensity on the polarization direction, i.e., a higher absorption when ***E*** is aligned in-plane compared to when it cants out-of-plane. The observed large asymmetry in the spectral intensity gives direct evidence that most of the Cu sites have holes occupying the $d_{x^2-y^2}$ orbital. This is unlike the case for the monoclinic phase of CuO where the hole is reported to occupy the e_g d_{z^2} orbital.[70] In essence, the results of polarized XAS in relation to the hole occupation at the Cu site are in agreement with the discussion based on tetragonal crystal field splitting of the *d* orbital energy levels as sketched in Fig. 8(b) and hence corroborate the tetragonal structure of CuO with $c/a > 1$.

B. Polarity induced atomic rearrangement in ultrathin SCO layers: plane versus chain-type structures

In this section, we demonstrate the experimental evidence for a structural transformation from planar to chain type structure upon reducing the SCO layer thickness. This process is realized via oxygen rearrangement which gives rise to a larger *c*-axis parameter for the modified structure as described in the Introduction [Fig. 3]. To illustrate this effect experimentally, we first present the results of the structural investigation using XRD on $((SCO)_m/(STO)_2)_{20}$ SLs where *m* equals the number of uc of SCO that varies from 3–16. The SLs show the signature of distinct satellite peaks which demonstrates the structural quality of the SLs.[48] In Fig. 9, we show the average *c*-axis lattice parameter as a function of the SCO thickness (*m*) in the SLs. The average *c*-axis lattice parameter is estimated from the $zero_{th}$ order satellite peak position. It is evident that the *c*-axis lattice parameter follows a decreasing trend as *m* increases, ranging from 3.84 to 3.36 Å for $((SCO)_3/(STO)_2)_{20}$ and $((SCO)_8/(STO)_2)_{20}$), respectively. However, for $m \geq 8$, the average *c*-axis lattice parameter remarkably levels out at a value close to the expected bulk SCO value ($a = b = 3.926$ Å and $c = 3.432$ Å).[43] The increase in the average *c*-axis lattice parameter at lower *m* suggests that the SCO layers undergo a gradual structural transformation to chain-type structure characterized by an elongation along the *c*-axis.

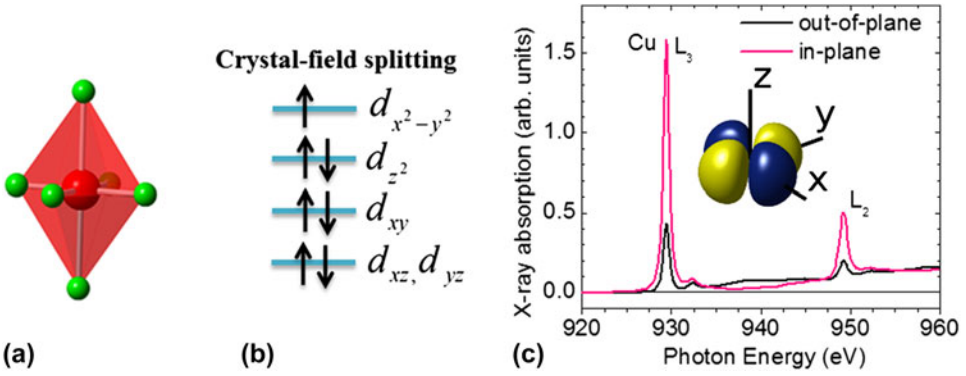


FIG. 8. Schematics for (a) elongated CuO_6 octahedron surrounding Cu ion, (b) relevant tetragonal crystal field split energy levels with electronic occupation of *d* orbitals at the Cu site (d_{xz} and d_{yz} shown as degenerate), and (c) polarized XA spectra for a tetragonal CuO film. The inset shows the schematic for the $d_{x^2-y^2}$ orbital where the hole at the Cu site is preferentially localized. [XAS spectra are originally from Ref. 20.]

https://doi.org/10.1557/jmr.2014.391 Published online by Cambridge University Press

To have further insight into the structural aspects precisely, we carried out an elaborate STEM investigation on a hybrid SL that consists of both plane and chain-type SCO layers separated by STO layers: $[((SCO)_8/(STO)_2/(SCO)_3/(STO)_2)_{10}]$. This particular SL structure was designed because it gives us an additional flexibility to directly compare the variation of the structural parameters as well as oxygen co-ordination with the SCO thickness variation in the same film. The *c*-axis lattice parameter for the $(SCO)_8$ layers as measured from HAADF-STEM is found to be 3.43(3) Å, which is 10% less than that of the $(SCO)_3$ layers (3.83(3) Å) present in the same SL structure.[48] This clearly illustrates the structural difference between $(SCO)_8$ and $(SCO)_3$ layers and strongly corroborates the findings based on XRD study. Since the arrangement of the oxygen atoms varies distinctly between chain and plane-type SCO layers, it is important to directly identify the oxygen ions on a local scale. For this reason, we carried out ABF-STEM imaging. Such a superimposed color map is presented in Fig. 10(a) with the low-angle scattering events (ABF-STEM) in green and the high-angle (HAADF-STEM) ones in red. The columns containing heavy elements (Sr, Cu, and Ti) together with oxygen atoms are visible as yellow (overlay of red and green) dots whereas the columns containing only oxygen atoms are visible in green. We clearly observe the oxygen columns between all the heavy atomic columns in $(SCO)_3$ and $(STO)_2$ layers, but no oxygen belonging to Sr-planes present in the $(SCO)_8$ layer. This directly confirms the planar-arrangement of the oxygen atoms in the $(SCO)_8$ layer as schematically shown in Fig. 3(a). However, the arrangement of the oxygen atoms in $(SCO)_3$ follows chain-type structure [Fig. 3(b)] having apical oxygen surrounding Cu ions. Simulated images assuming these structures are shown to guide the reader in interpreting the subtle differences visible in Fig. 10(a). For the sake of clarity, we also show ABF line profile [Figs. 10(b) and

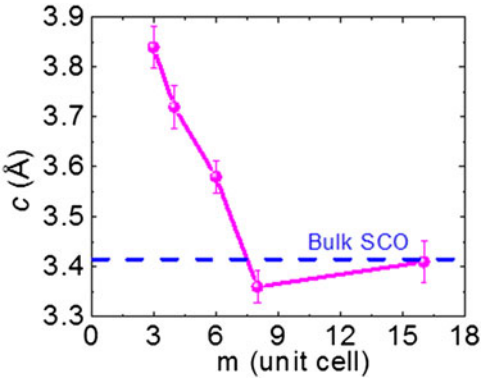


FIG. 9. Average *c*-axis lattice parameter as a function of SCO thickness for $((SCO)_m/(STO)_2)_{20}$ SLs. The horizontal dashed-line marks the reported bulk *c*-axis lattice parameter for IL SCO. [Data taken from Ref. 48.]

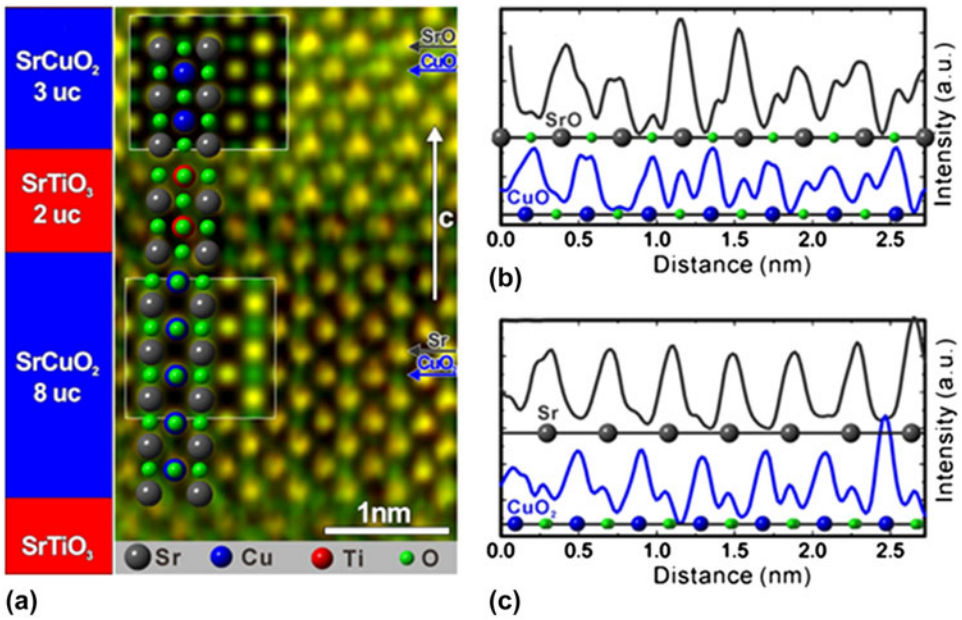


FIG. 10. (a) Combined color map from the simultaneously acquired ADF (red) and inverted intensity ABF image (green). The yellow peaks indicate the heavy elements (Sr, Cu, and Ti) while the green peaks highlight the light elements (O). A clear structural difference is seen between the SCO_3 (chain) and the SCO_8 (planar) layer, which is confirmed by comparing to simulated images (insets) in the respective layers. A structural model is overlaid. (b) ABF line profile through the SrO plane (gray) and CuO plane (blue) in the $(SCO)_3$ layer as indicated by gray and blue arrows. (c) ABF line profile through the Sr plane (gray) and CuO_2 plane (blue) in the $(SCO)_8$ layer as indicated by gray and blue arrows. The oxygen positions are marked by green dots and appear as extra peaks in the ABF signal. [Image (a) is taken from Ref. 48.]

https://doi.org/10.1557/jmr.2014.391 Published online by Cambridge University Press

10(c)] through the SrO, CuO, Sr, and CuO_2 planes that indicate the oxygen positions (marked by green dots) and appear as extra peaks in the ABF signal.

Based on structural investigation, it is evident that there occurs a transformation from plane to chain-type structure upon reducing the SCO thickness. To know how the Cu electronic structure and symmetry of the unoccupied Cu 3*d* orbital get modified when SCO undergoes a structural transformation to chain-type structure, we performed XA spectroscopy using linearly polarized x-rays. In Fig. 11, we show XA spectra at the Cu $L_{2,3}$ edges for $((SCO)_3/(STO)_2)_{10}$ and $((SCO)_8/(STO)_2)_5$ SLs with the ***E*** vector aligned in-plane and canted out-of-plane relative to the *c*-axis of the SL. For $((SCO)_8/(STO)_2)_5$ SL [Fig. 11(a)], we observe a strong dependence of the spectral intensity on the polarization direction, i.e., a stronger absorption when ***E*** is aligned in-plane compared to that when it cants out-of-plane, respectively. Such asymmetry indicates that most of the Cu sites have holes occupying the $d_{x^2-y^2}$ orbital. Besides Cu L_3 white light transition, a second significantly weaker peak is observed ~4.6 eV higher in energy corresponding to a small content of monovalent Cu.[68,69,71] However for $((SCO)_3/(STO)_2)_{10})$ SL [Fig. 11(b)], the absorption peak intensity and spectral shape are found to be nearly identical irrespective of the orientation of the ***E*** and no linear dichroism is observed. This indicates that both $d_{x^2-y^2}$ and d_{z^2} orbitals are equally populated and such observation could be directly linked to the presence of apical oxygen in the chain-type SCO layers unlike the planar one. Moreover, the Cu spectra are characterized by two weak peaks, namely the monovalent Cu peak and a shoulder at ~1.4 eV above the main peak. The shoulder above ~1.4 eV the main peak position is assigned to $3d^{10}L$ final state configuration, where *L* denotes a 2*p* hole at the oxygen sites arising out of Cu3*d*–O2*p* hybridization.[58,67–69] XAS results provide profound difference in relation to hole occupation at the Cu site between $[(SCO)_8/(STO)_2)]_{10}$ and $[((SCO)_3/(STO)_2)_{10}]$ SLs and this goes in line with our finding of apical oxygen ions surrounding the Cu ion in $(SCO)_3$ layers. One might think that there could be additional factors such as oxygen defects and/or the interfacial oxygen[58,72,73] (that can give rise to the apical site for Cu ions), which can contribute to the XA spectra. However, these secondary effects cannot fully account for such a marked difference. To further elucidate this issue and justify that the observed phenomena are not an interfacial effect, we examined and compared the structural parameters between two bare SCO single layers, where one is 3 uc thick and the other is 9 uc thick, by performing the in situ XPD study.[59] XPD is a highly suitable technique that can be used to derive the structural information of ultrathin films. In this process, x-rays of sufficient energy are illuminated on the sample to excite the core electrons of atoms within the sample and the intensity of emitted photoelectron is usually studied either by changing the azimuthal or polar angle (see Fig. 12). The photoelectrons scattered from the neighboring surrounding atoms can interfere and give rise to the diffraction pattern. Therefore, using this technique one can study the nature of surrounding of each element in the sample. High-resolution XPD scans for Cu-2*p*, Sr-3*d*, and O-1*s* electrons of both SCO films are depicted in Fig. 12 as a function of θ (emission angle/polar angle). A clear shift in θ peak positions in the O 1*s* and Sr 3*d*

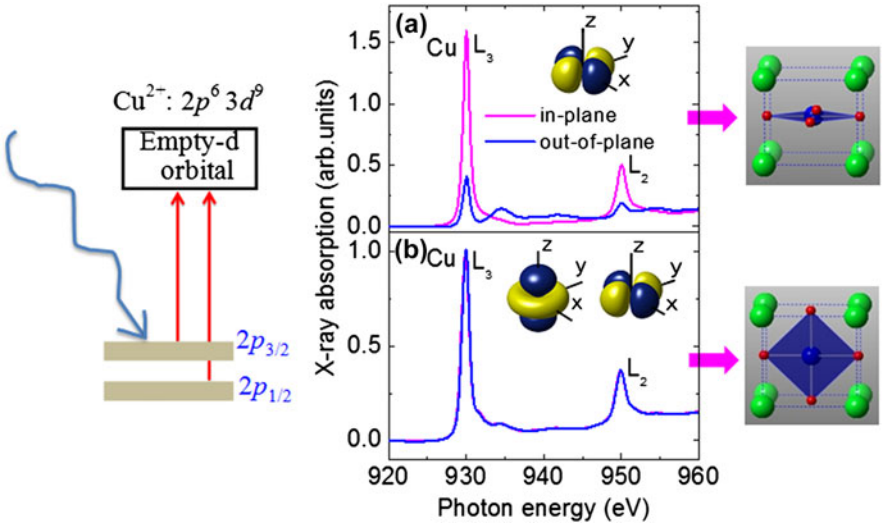


FIG. 11. Polarized XA spectra for (a) $((SCO)_8/(STO)_2)_5$ and (b) $((SCO)_3/(STO)_2)_{10}$ SLs. The insets show schematics for the *d*-orbitals where the hole is preferentially localized. The left hand side shows a sketch for the XAS process for $2p \rightarrow 3d$ transition. The right hand side schematics represent the corresponding plane and chain-type configurations for $(SCO)_8$ and $(SCO)_3$ layers, respectively (red and blue spheres correspond to oxygen and copper, respectively). [XAS spectra are originally from Ref. 48.]

https://doi.org/10.1557/jmr.2014.391 Published online by Cambridge University Press

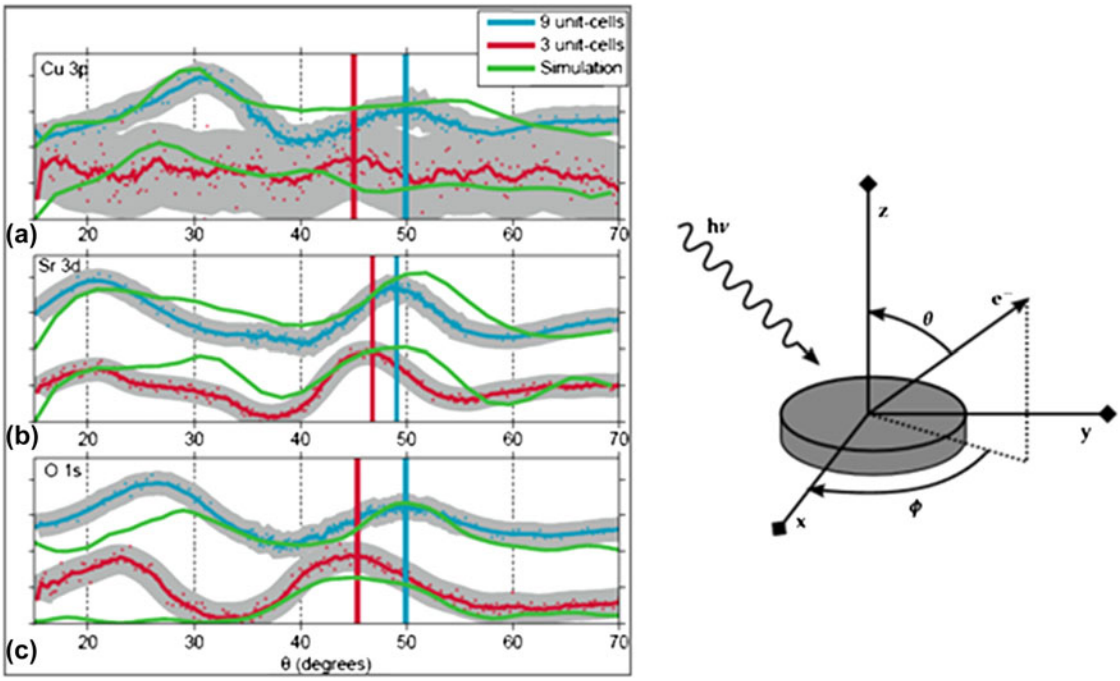


FIG. 12. XPD pattern (both experiment and simulation) for 3 and 9 uc thick SCO films. θ scans are shown for (a) Cu-3*p*, (b) Sr-3*d*, and (c) O-1*s*. The dots are measured data points, similar colored solid lines are acquired by applying a 9-point moving average. Multiple scattering electron diffraction simulation results are shown in green. The right-hand image schematically indicates the XPD measurement geometry, where θ is a polar angle and Φ is an azimuthal angle. [Image is taken from Ref. 59.]

scans is observed when compared between 3 and 9 uc SCO films, indicating comparatively larger *c*-axis lattice parameter for 3 uc SCO layer. For clarity, the peak positions are indicated by vertical lines. From the analysis of XPD spectra, we find that the *c*-axis lattice parameter for 3 uc SCO is longer by ~0.5 Å than that of the 9 uc SCO layer and this is in well agreement with our findings based on the study of SCO/STO SLs. Hence, it clearly suggests that the oxygen rearrangement occurs well within the SCO layer. A detailed discussion about the analysis and interpretation of XPD results on SCO thin films can be found from the recent published work by Kuiper and co-workers.[59] Had the chain-type transformation been only an interfacial effect, we would not have noticed an increase in *c*-axis lattice parameter corresponding to chain-type structure in the bare 3 uc single layer SCO film. Thus, we clearly view a thickness-dependent structural transformation via oxygen-rearrangement throughout the bulk of the SCO layer. Our finding does not agree with the recent report by Aruta et al.[73] where they hypothesize on another mechanism via oxygen redistribution in the interfacial planes, to explain their experimental results studied using hard x-ray photoelectron spectroscopy on ($CaCuO_2$/STO) SLs. The differences could be related to different oxidizing growth conditions used and moreover the system investigated by Aruta et al.[73] is as well different than that of us.

IV. SUMMARY AND CONCLUSIONS

We have demonstrated novel routes by which the oxygen sublattice in ultrathin films of two ideal cuprate members (CuO and SCO) can be rearranged in a controlled way. By imposing epitaxial strain from the STO substrate to ultrathin CuO layers, we illustrate the stabilization of tetragonal rocksalt type CuO structure, which is very much different from its bulk counterpart. Specifically, the findings based on STEM study directly reveal that the unit cell of ultrathin CuO layers is elongated along the *c*-axis ($c/a \sim 1.34$) and has a Cu–O–Cu bond angle, $\varphi = 180 \pm 2°$. Structural findings are complemented with polarized XAS experiments that clearly reveals the $d_{x^2-y^2}$ hole symmetry at Cu site and this goes in line considering the tetragonal crystal field splitting of the *d* orbitals. The direct evidence for the existence of a high-symmetry tetragonal CuO, a benchmark system, will encourage experiments to probe its novel electronic property and trigger doping experiments in the quest for high-T_c superconductivity. In case of SCO thin films, we demonstrate the possibility for a structural transformation (plane to chain-type), where the geometry of CuO_4 plaquettes is rotated by 90° at ultralow thickness limit. This phenomenon turns out to be a direct response to electrostatic instability associated with IL

https://doi.org/10.1557/jmr.2014.391 Published online by Cambridge University Press

polar cuprates. The modified chain-type structure acquires oxygen in the Sr plane providing an apical site for Cu ion, very similar to what is generally observed for chain type Cu–O blocks in high-T_c superconducting materials. A detailed structural study based on XRD, XPD, and STEM clearly reveals an increase in *c*-axis lattice parameter by ~0.5 Å and the presence of oxygen ions in the Sr-plane for ultrathin SCO films contrary to their bulk counterpart. A combination of ABF and ADF imaging has been used to directly visualize the change in oxygen positions as the thickness of SCO layer is varied. Structural findings are also complemented with polarized XAS experiments that clearly distinguishes the plane and chain-type SCO structures with respect to hole distribution at Cu-site. For plane-type SCO structure, the hole is localized in $d_{x^2-y^2}$ orbital. However, for chain-type SCO layers, both $d_{x^2-y^2}$ and d_{z^2} orbitals are equally populated. The presence of apical oxygen surrounding the Cu ion in the chain-type SCO layer provides the basis for having higher density of out-of-plane holes as compared to the planar case. We strongly believe that our experimental findings on SCO ultrathin films will trigger activities in making novel artificial Cu-based high-T_c superconductors, where the charge reservoir layer can be constituted by the ultrathin SCO layers having apical oxygen. Artificial cuprate structures having altered chain and plane-type layers (the basic building blocks in cuprates) will be model systems to explore interesting electronic properties, with specific aim to look for enhanced superconducting properties. Moreover, since we know that the magnetism in cuprates strongly depends upon oxygen co-ordination surrounding the Cu ion and Cu–O–Cu angle, it will be very much encouraging to investigate the associated magnetic property that can emerge from these novel i.e., both rocksalt type CuO as well as chain-type SCO structures. It has been brought to our attention that an angle-resolved photoemission spectroscopy of tetragonal CuO has been published by Moser *et al.*[74]

ACKNOWLEDGMENTS

The authors would like to acknowledge fruitful discussions with Y. Takamura, J. Verbeeck, H. Tan, G. Rijnders, H. Molegraaf, W. Siemons, B. Kuiper, and Z. Zhong. D.S. and G.K gratefully acknowledge financial support from AFOSR and EOARD project (project number: FA8655-10-1-3077).

REFERENCES

1. G.J.H.M. Rijnders, G. Koster, D.H.A. Blank, and H. Rogalla: In situ monitoring during pulsed laser deposition of complex oxides using reflection high energy electron diffraction under high oxygen pressure. *Appl. Phys. Lett.* **70**, 1888 (1997).
2. I. Bozovic and J.N. Eckstein: Analysis of growing films of complex oxides by RHEED. *MRS Bull.* **20**, 32 (1995).
3. H.N. Lee, H.M. Christen, M.F. Chisholm, C.M. Rouleau, and D.H. Lowndes: Strong polarization enhancement in asymmetric three-component ferroelectric superlattices. *Nature* **433**, 395 (2005).
4. J. Chakhalian, J.W. Freeland, G. Srajer, J. Strempfer, G. Khaliullin, J.C. Cezar, T. Charlton, R. Dalgliesh, C. Bernhard, G. Cristiani, H.U. Habermeier, and B. Keimer: Magnetism at the interface between ferromagnetic and superconducting oxides. *Nat. Phys.* **2**, 244 (2006).
5. J. Chakhalian, J.W. Freeland, H.U. Habermeier, G. Cristiani, G. Khaliullin, M. van Veenendaal, and B. Keimer: Orbital reconstruction and covalent bonding at an oxide interface. *Science* **318**, 1114 (2007).
6. D. Samal, C. Shivakumara, and P.S. Anil Kumar: Magnetotransport study on $La_{0.5}Sr_{0.5}CoO_{3-\delta}/YBa_2Cu_3O_{7-\delta}/La_{0.7}Ca_{0.3}MnO_{3-\delta}$ tri-layer system. *Phys. Rev. B* **77**, 094510 (2008).
7. H.Y. Hwang, Y. Iwasa, M. Kawasaki, B. Keimer, N. Nagaosa, and Y. Tokura: Emergent phenomena at oxide interfaces. *Nat. Mater.* **11**, 102 (2012).
8. J. Mannhart and D.G. Schlom: Oxide interfaces–An opportunity for electronics. *Science* **327**, 1607 (2010).
9. P. Zubko, S. Gariglio, M. Gabay, P. Ghosez, and J-M. Triscone: Interface physics in complex oxide heterostructures. *Annu. Rev. Condens. Matter Phys.* **2**, 141 (2011).
10. S.J. May, J.W. Kim, J.M. Rondinelli, E. Karapetrova, N.A. Spaldin, A. Bhattacharya, and P.J. Ryan: Quantifying octahedral rotations in strained perovskite oxide films. *Phys. Rev. B* **82**, 014110 (2010).
11. J. He, A. Borisevich, S.V. Kalinin, S.J. Pennycook, and S.T. Pantelides: Control of octahedral tilts and magnetic properties of perovskite oxide heterostructures by substrate symmetry. *Phys. Rev. Lett.* **105**, 227203 (2010).
12. R. Aso, D. Kan, Z. Shimakaw, and H. Kurata: Atomic level observation of octahedral distortions at the perovskite oxide heterointerface. *Sci. Rep.* **3**, 2214 (2013).
13. J.M. Rondinelli, S.J. May, and J.W. Freeland: Control of octahedral connectivity in perovskite oxide heterostructures: An emerging route to multifunctional materials discovery. *MRS Bull.* **37**, 261 (2012).
14. J.M. Rondinelli and N.A. Spaldin: A structure and properties of functional oxide thin films: Insights from electronic-structure calculations. *Adv. Mater.* **23**, 3363 (2011).
15. H.Y. Hwang, S-W. Cheong, P.G. Radaelli, M. Marezio, and B. Batlogg: Lattice effects on the magnetoresistance in doped $LaMnO_3$. *Phys. Rev. Lett.* **75**, 914 (1995).
16. M.L. Medard: Structural, magnetic and electronic properties of $RNiO_3$ perovskites (R = rare earth). *J. Phys.: Condens. Matter* **9**, 1679 (1997).
17. F.J. Wong, S-H. Baek, R.V. Chopdekar, V.V. Mehta, H.W. Jang, C-B. Eom, and Y. Suzuki: Metallicity in $LaTiO_3$ thin films induced by lattice deformation. *Phys. Rev. B* **81**, 161101 (2010).
18. H. Boschker, J. Kautz, E.P. Houwman, W. Siemons, D.H.A. Blank, M. Huijben, G. Koster, A. Vailionis, and G. Rijnders: High-temperature magnetic insulating phase in ultrathin $La_{0.67}Sr_{0.33}MnO_3$ films. *Phys. Rev. Lett.* **109**, 157207 (2012).
19. E. Bousquet, M. Dawber, N. Stucki, C. Lichtensteiger, P. Hermet, S. Gariglio, J-M. Triscone, and P. Ghosez: Improper ferroelectricity in perovskite oxide artificial superlattices. *Nature* **452**, 732 (2008).
20. D. Samal, H. Tan, Y. Takamura, W. Siemons, J. Verbeeck, G.V. Tendeloo, E. Arenholz, C.A. Jenkins, G. Rijnders, and G. Koster: Direct structural and spectroscopic investigation of ultrathin films of tetragonal CuO: Six-fold co-ordinated copper. *Europhys. Lett.* **105**, 17003 (2014).

https://doi.org/10.1557/jmr.2014.391 Published online by Cambridge University Press

21. W. Siemons, G. Koster, D.H.A. Blank, R.H. Hammond, T.H. Geballe, and M.R. Beasley: Tetragonal CuO: End member of the 3d transition metal monoxides. *Phys. Rev. B* **79**, 195122 (2009).
22. X. Rocquefelte, X.K. Schwarz, and P. Blaha: Theoretical investigation of the magnetic exchange interactions in copper(II) oxides under chemical and physical pressures. *Sci. Rep.* **2**, 759 (2012).
23. M. Salluzzo, C. Aruta, G. Ausanio, A. D'Agostino, and U. Scotti di Uccio: Effect of strain on the structure and critical temperature in superconducting Nd-doped $YBa_2Cu_3O_{7-\delta}$. *Phys. Rev. B* **66**, 184518 (2002).
24. M. Salluzzo, G.M. de Luca, D. Marrè, M. Putti, M. Tropeano, U. Scotti di Uccio, and R. Vaglio: Thickness effect on the structure and superconductivity of $Nd_{1.2}Ba_{1.8}Cu_3O_z$ epitaxial films. *Phys. Rev. B* **72**, 134521 (2005).
25. T. Haage, J. Zegenhagen, H-U. Habermeier, and M. Cardona: Nucleation mechanism of $YBa_2Cu_3O_{7-\delta}$ on $SrTiO_3$(001). *Phys. Rev. Lett.* **80**, 4225 (1998).
26. L.F. Mattheiss: Electronic structure of the 3d transition-metal monoxides. I. Energy-band results. *Phys. Rev. B* **5**, 290 (1972).
27. K. Terakura, T. Oguchi, A.R. Williams, and J. Kübler: Band theory of insulating transition-metal monoxides: Band-structure calculations. *Phys. Rev. B* **30**, 4734 (1984).
28. W.A. Harrison: Heisenberg exchange in the magnetic monoxides. *Phys. Rev. B* **76**, 054417 (2007).
29. G. Fischer, M. Däne, A. Ernst, P. Bruno, M. Lüders, Z. Szotek, W. Temmerman, and W. Hergert: Exchange coupling in transition metal monoxides: Electronic structure calculations. *Phys. Rev. B* **80**, 014408 (2009).
30. B. Yang, T. Thurston, T.J. Tranquada, and G. Shirane: Magnetic neutron scattering of single-crystal cupric oxide. *Phys. Rev. B* **39**, 4343 (1989).
31. T. Kimura, Y. Sekio, H. Nakamura, T. Siegrist, and A.P. Ramirez: Cupric oxide as an induced-multiferroic with high-T_C. *Nat. Mater.* **7**, 291 (2008).
32. X. Chen, C.L. Fu, C. Franchini, and R. Podloucky: Hybrid density-functional calculation of the electronic and magnetic structures of tetragonal CuO. *Phys. Rev. B* **80**, 094527 (2009).
33. G. Peralta, D. Puggioni, A. Filippetti, and V. Fiorentini: Jahn-Teller stabilization of magnetic and orbital ordering in rocksalt CuO. *Phys. Rev. B* **80**, 140408 (2009).
34. K.S. Rabinovich, L.L. Samoilenko, A.S. Zhuravleva, and A.G. Shneider: Magnetic properties of high-symmetry CuO. *Appl. Phys. Lett.* **104**, 182406 (2014).
35. J. Bednorz and K. Muller: Perovskite-type oxides—The new approach to high-T_c superconductivity. *Rev. Mod. Phys.* **60**, 585 (1988).
36. P.M. Grant: Electronic properties of rocksalt copper monoxide: A proxy structure for high temperature superconductivity. *J. Phys.: Conf. Ser.* **129**, 012042 (2008).
37. A. Ohtomo and H.Y. Hwang: A high-mobility electron gas at the $LaAlO_3/SrTiO_3$ heterointerface. *Nature* **427**, 423 (2004).
38. S. Thiel, G. Hammerl, A. Schmehl, C.W. Schneider, and J. Mannhart: Tunable quasi-two dimensional electron gases in oxide heterostructures. *Science* **313**, 1942 (2006).
39. N. Reyren, S. Thiel, A.D. Caviglia, L. Fitting Kourkoutis, G. Hammerl, C. Richter, C.W. Schneider, T. Kopp, A.S. Rüetschi, D. Jaccard, M. Gabay, D.A. Muller, J-M. Triscone, and J. Mannhart: Superconducting interfaces between insulating oxides. *Science* **317**, 119 (2007).
40. J.A. Bert, B. Kalisky, C. Bell, M. Kim, Y. Hikita, H.Y. Hwang, and K.A. Moler: Direct imaging of the coexistence of ferromagnetism and superconductivity at the $LaAlO_3/SrTiO_3$ interface. *Nat. Phys.* **7**, 767 (2011).
41. A. Brinkman, M. Huijben, M. van Zalk, J. Huijben, U. Zeitler, J.C. Maan, W.G. van der Wiel, G. Rijnders, D.H.A. Blank, and H. Hilgenkamp: Magnetic effects at the interface between non-magnetic oxides. *Nat. Mater.* **6**, 493 (2007).
42. A.J. Millis and D.G. Schlom: Electron-hole liquids in transition-metal oxide heterostructures. *Phys. Rev. B* **82**, 073101 (2010).
43. M. Takano, Y. Takeda, H. Okada, M. Miyamoto, and T. Kusaka: $ACuO_2$ (A: alkaline earth) crystallizing in a layered structure. *Phys. C* **159**, 375 (1989).
44. G. Koster, A. Brinkman, H. Hilgenkamp, A.J.H.M. Rijnders, and D.H.A. Blank: High-T_c superconducting thin films with composition control on a sub-unit cell level; the effect of the polar nature of the cuprates. *J. Phys.: Condens. Matter* **20**, 264007 (2009).
45. H. Matsueda, N. Bulut, T. Tohyama, and S. Maekawa: Temperature dependence of spinon and holon excitations in one-dimensional Mott insulators. *Phys. Rev. B* **72**, 75136 (2005).
46. B.J. Kim, H. Koh, E. Rotenberg, S-J. Oh, H. Eisaki, N. Motoyama, S. Uchida, T. Tohyama, S. Maekawa, Z-X. Shen, and C. Kim: Distinct spinon and holon dispersions in photoemission spectral functions from one-dimensional $SrCuO_2$. *Nat. Phys.* **2**, 397 (2006).
47. C. Kim, A.Y. Matsuura, Z.X. Shen, N. Motoyama, H. Eisaki, S. Uchida, T. Tohyama, and S. Maekawa: Observation of spin-charge separation in one-dimensional $SrCuO_2$. *Phys. Rev. Lett.* **77**, 4054 (1996).
48. D. Samal, H. Tan, H. Molegraaf, B. Kuiper, W. Siemons, S. Bals, J. Verbeeck, G.V. Tendeloo, Y. Takamura, E. Arenholz, C.A. Jenkins, G. Rijnders, and G. Koster: Experimental evidence for oxygen sub-lattice control in polar infinite-layer $SrCuO_2$. *Phys. Rev. Lett.* **111**, 096102 (2013).
49. G.E.S. Kikkawa, F. Kanamaru, and Y. Miyamoto: Structural, electrical and magnetic studies of infinite-layered $Sr_{1-x}La_xCuO_2$ superconductor. *Phys. C* **196**, 271 (1992).
50. M. Azuma, Z. Hiroi, M. Takano, Y. Bando, and Y. Takeda: Superconductivity at 110 K in the infinite-layer compound $(Sr_{1-x}Ca_x)_{1-y}CuO_2$. *Nature* **356**, 775 (1992).
51. M.G. Smith, A. Manthiram, J. Zhou, J.B. Goodenough, and J.T. Markert: Electron-doped superconductivity at 40 K in the infinite-layer compound $Sr_{1-y}Nd_yCuO_2$. *Nature* **351**, 549 (1991).
52. Z. Zhong, G. Koster, and P.J. Kelly: Prediction of thickness limits of ideal polar ultrathin films. *Phys. Rev. B* **85**, 121411 (2012).
53. J. Goniakowski, C. Noguera, and L. Giordano: Prediction of uncompensated polarity in ultrathin films. *Phys. Rev. Lett.* **98**, 205701 (2007).
54. J. Goniakowski, C. Noguera, and L. Giordano: Using polarity for engineering oxide nanostructures: Structural phase diagram in free and supported MgO (111) ultrathin films. *Phys. Rev. Lett.* **93**, 215702 (2004).
55. A. Harrison, E.A. Kraut, J.R. Waldrop, and R.W. Grant: Polar heterojunction interfaces. *Phys. Rev. B* **18**, 4402–4410 (1978).
56. D. Samal, Y. Takamura, G. Rijnders, and G. Koster: Tailoring superconducting properties in infinite-layer based cuprate heterostructures. (To be published).
57. M. Huijben, G. Koster, M.K. Kruize, S. Wenderich, J. Verbeeck, S. Bals, E. Slooten, B. Shi, H.J.A. Molegraaf, J.E. Kleibeuker, S. van Aert, J.B. Goedkoop, A. Brinkman, D.H.A. Blank, M.S. Golden, G. van Tendeloo, H. Hilgenkamp, and G. Rijnders: Defect engineering in oxide heterostructures by enhanced oxygen surface exchange. *Adv. Funct. Mater.* **23**, 5240 (2013).
58. D. Di Castro, M. Salvato, A. Tebano, D. Innocenti, C. Aruta, W. Prellier, O.I. Lebedev, I. Ottaviani, N.B. Brookes, M. Minola, M. Moretti Sala, C. Mazzoli, P.G. Medaglia, G. Ghiringhelli, L. Braicovich, M. Cirillo, and G. Balestrino: Occurrence of a high-temperature superconducting phase in $(CaCuO_2)_n/(SrTiO_3)_m$ superlattice. *Phys. Rev. B* **86**, 134524 (2012).

https://doi.org/10.1557/jmr.2014.391 Published online by Cambridge University Press

59. B. Kuiper, D. Samal, D.H.A. Blank, J.E. ten Elshof, G. Rijnders, and G. Koster: Control of oxygen sub-lattice structure in ultra-thin $SrCuO_2$ films studied by x-ray photoelectron diffraction. *APL Mater.* **1**, 042113 (2013).
60. M. Cyrot and D. Pavuna: *Introduction to Superconductivity and High-T_c Materials* (World Scientific, Singapore, 1992).
61. G. Balestrino, S. Martellucci, P.G. Medaglia, A. Paoletti, and G. Petrocelli: Dependence of the critical temperature on n in $(BaCuO_2)_2/(CaCuO_2)_n$ superlattices. *Phys. Rev. B* **58**, R8925 (1998).
62. G. Balestrino, G. Pasquini, and A. Tebano: Structural features of $(Ba_2Cu_2O_{4+x})/(CaCuO_2)_n$ superconducting oxide superlattices with ultrathin individual layers. *Phys. Rev. B* **62**, 1421 (2000).
63. D.P. Norton, B.C. Chakoumakos, J.D. Budai, D.H. Lowndes, B.C. Sales, J.R. Thompson, and D.K. Christen: Superconductivity in $SrCuO_2$-$BaCuO_2$ superlattices: Formation of artificially layered superconducting materials. *Science* **265**, 2074 (1994).
64. A. Rosenauer and M. Schowalter: *STEMSIM-A New Software Tool for Simulation of STEM HAADF: Microscopy of Semiconducting Materials (MSM) Conference, 2007*, Vol. **120**, Springer, Netherlands, 2008; p. 169.
65. S.D. Findlay, N. Shibata, H. Sawada, E. Okunishi, Y. Kondo, and Y. Ikuhara: Dynamics of annular bright field imaging in scanning transmission electron microscopy. *Ultramicroscopy* **110**, 903 (2010).
66. D.D. Sarma, O. Strebel, C.T. Simmons, U. Neukirch, G. Kaindl, R. Hoppe, and H.P. Muller: Electronic structure of high-T_c superconductors from soft-x-ray absorption. *Phys. Rev. B* **37**, 9784 (1988).
67. C.T. Chen, L.H. Tjeng, J. Kwo, H.L. Kao, P. Rudolf, F. Sette, and R.M. Fleming: Out-of-plane orbital characters of intrinsic and doped holes in $La_{2-x}Sr_xCuO_4$. *Phys. Rev. Lett.* **68**, 2543 (1992).
68. D.G. Hawthorn, K.M. Shen, J. Geck, D.C. Peets, H. Wadati, J. Okamoto, S-W. Huang, D.J. Huang, H-J. Lin, J.D. Denlinger, R. Liang, D.A. Bonn, W.N. Hardy, and G.A. Sawatzky: Resonant elastic soft x-ray scattering in oxygen-ordered $YBa_2Cu_3O_{6+\delta}$. *Phys. Rev. B* **84**, 075125 (2011).
69. M. Salluzzo, G. Ghiringheli, N.B. Brookes, G.M. De Luca, F. Fracassi, and R. vaglio: Superconducting-insulator transition driven by out of plane carrier localization in $Nd_{1.2}Ba_{1.8}Cu_3O_{7+x}$. *Phys. Rev. B* **75**, 054519 (2007).
70. A. Filippetti and V. Fiorentini: Magnetic ordering in CuO from first principles: A cuprate antiferromagnet with fully three-dimensional exchange interactions. *Phys. Rev. Lett.* **95**, 086405 (2005).
71. N. Nücker, E. Pellegrin, P. Schweiss, E. Sohmen, J. Fink, S.L. Molodtsov, C.T. Simmons, M. Domke, G. Kaindl, W. Frientrup, C.T. Chen, A. Erb, and G. Müller-Vogt: Site-specific and doping-dependent electronic structure of $YBa_2Cu_3O_x$ probed by O 1*s* and Cu 2*p* x-ray-absorption spectroscopy. *Phys. Rev. B* **51**, 8529 (1995).
72. C. Aruta, G. Ghiringhelli, C. Dallera, F. Fracassi, P.G. Medaglia, A. Tebano, N.B. Brookes, L. Braicovich, and G. Balestrino: Hole redistribution across interfaces in superconducting cuprate superlattices. *Phys. Rev. B* **78**, 205120 (2008).
73. C. Aruta, C. Schlueter, T.L. Lee, D. Di Castro, D. Innocenti, A. Tebano, J. Zegenhagen, and G. Balestrino: Interface reconstruction in superconducting $CaCuO_2/SrTiO_3$ superlattices: A hard x-ray photoelectron spectroscopy study. *Phys. Rev. B* **78**, 155145 (2013).
74. S. Moser, L. Moreschini, H.-Y. Yang, D. Innocenti, F. Fuchs, N.H. Hansen, Y.J. Chang, K.S. Kim, A.L. Walter, A. Bostwick, E. Rotenberg, F. Mila, and M. Grioni: Angle-Resolved Photoemission Spectroscopy of Tetragonal CuO: Evidence for Intralayer Coupling Between Cupratelike Sublattices. *Phys. Rev. Lett.* **113**, 187001 (2014).

https://doi.org/10.1557/jmr.2014.391 Published online by Cambridge University Press